Answers to Reviewer #1

Specific comments

Q1: Title: The title is misleading as it suggests a link between the weather conditions and the bridge collapse.

A1: We kindly disagree with the reviewer's observation that the title suggests there is an established connection between the collapse and the weather conditions. It is a fact that these weather conditions were observed during the bridge collapse. Hence, we wrote "…weather conditions during the collapse…" and not weather conditions that caused or potentially caused the collapse. Therefore, we have left the title as it was in the original manuscript.

Q2: 41: While the authors state that there is lightning in the picture, the lightning was not detected by the network (as described in Sect. 3.1).

A2: The lightning was detected by the network indeed. Fig. 1a is taken from the west with respect to the bridge and the photo shows the east. This is indicated in Fig. 1b because if north is left and south is right, east is forward. Now, in Fig. 8 you can clearly see that lightning strikes were detected to the east of the bridge; therefore, everything is perfectly coherent.

Q3: 53-56: This may be the case but the presented data are not really suitable to quantify the role of weather in the collapse.

A3: We struggle to understand the reviewer's comments on why it is not good that we did not explicitly demonstrate that the weather caused the collapse. As we explained in our answer to the general comment, in order to quantify the wind actions on the bridge, the person would have to carry out a detailed structural analysis study. However, such a study is impossible to be conducted if there is no information about the wind. Hence, this study documents and explores the wind conditions in the thunderstorm that was present during the collapse.

Q4: 59-62: The large HyMeX programme should be mentioned in this context.

A4: The paper by Drobinski et al. (2013) will be included in the citation list. Thank you.

Q5: 62-66: In my opinion it is not necessary to describe the previous storm in so much detail as it is not decisive for the study.

A5: This description will be shortened to a single sentence in the revised manuscript.

Q6: 76-78: The comparison between downbursts and the ABL is not adequate. The statement implies that the ABL wind is correctly represented in models. Models still fail to correctly represent the ABL conditions in particular over complex terrain. As the scale of downbursts is not resolved by NWP grid spacing, it is not surprising that the models fail to represent them.

A6: This sentence does not mention numerical modelling—the NWP or other modelling—of either ABL or downburst winds. We simply state that the dynamics of downbursts are more complex that the dynamics of ABL winds.

Q7: 79-86: Confine to the most relevant studies.

A7: This section will be significantly reduced. Only a sample of few relevant studies for field measurements of downburst winds in the Ligurian and the northern Tyrrhenian Sea will be included. The references to Google Scholar indexing of downburst-related studies will be also omitted in the new manuscript.

Q8: 101-106: The detailed description of aircraft crashes is not relevant.

A8: This part will be removed from the revised manuscript.

Q9: 111: This is not a scientific objective.

A9: We kindly disagree with the reviewer. As we explained in our answer to the general comment above, this objective corroborates with the scope of this journal. The paper investigates a severe natural phenomenon that occurred during a hazard. It is certainly not illogical to suspect a connection between high impact weather (thunderstorm downburst) and bridge collapse, without attempting to dis(prove) such a connection. This bridge collapse is such an enormous event that will probably be investigated in many studies and it is impossible to lump together all different research approaches in one paper. While we are planning to analyze this event from different perspectives too (some of them being similar to what the reviewer suggested here), these studies are beyond this paper. The present paper rigorously describes the weather conditions during the collapse, as well as the contributing factors for this severe weather.

However, we will add the sentence that the future study that we are currently working on will present a detailed three-dimensional reconstruction of this flow field using Doppler lidar and radar observations. This study is still ongoing and the scope of such a paper is probably not adequate for this journal.

Q10: 115ff: The model simulations are not presented in a way that they complement the observational analysis.

A10: The numerical simulations were conducted in order to investigate the predictability of this thunderstorm event in an operational weather forecasting model. We opted not to use any research-oriented WRF configurations, but instead, we wanted to assess the accuracy of the operational weather forecast of this weather event in the given 1-h interval around the bridge collapse.

In addition to the original manuscript version, we have now carried out a simulation including the data assimilation on the IFS driven forecast, namely WRF-IFS-DA. This will be added to the discussion in the revised paper. This prediction in comparison to the WRF-IFS experiment shows two main advantages: (1) wind peaks up to 12–13 m s^{-1} over the 8 wind stations used in the study; and (2) the thunderstorm event occurring one hour closer to the observed wind peaks. The forecast improvements are due to a better modelling of the observed thunderstorm activity (Figure A) close to Genoa in the late morning of 14 August 2018. Therefore, the WRF-IFS-DA simulation gave better results than the other runs. The WRF-IFS-DA predicted the storms in the period 11–12 UTC and produced the maximum wind gusts around 15–20 m s^{-1} (Figure B). The modelled storm was located only 8–10 km away from the location of anemometers and the location error is only 4–6 times the grid spacing (Grasso 2000). Indeed, this is a very accurate simulation result.
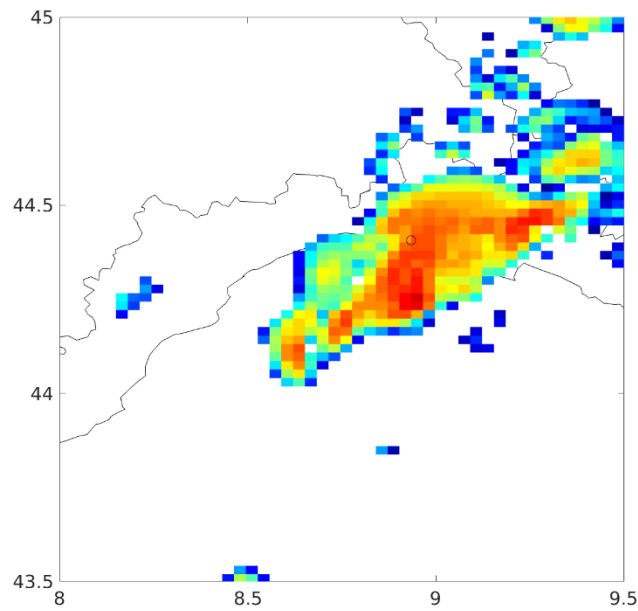
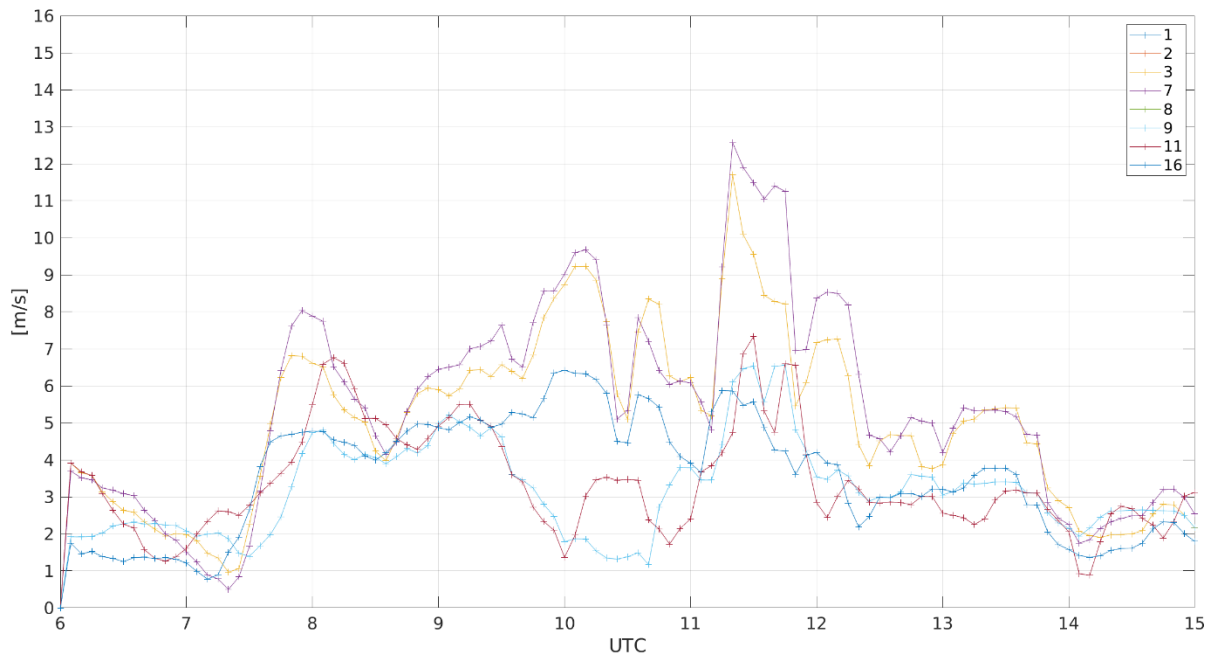Figure A. VMI map from WRF-IFS-DA run at 11:30 UTC.

Figure B. Maximum 5-min wind speeds at 10 m above ground from the WRF-IFS-DA simulation at the locations of eight anemometers in the Port of Genoa.

All considered, it is now even more relevant the role of the numerical results to complement the observational analysis, in particular after the additional effort to make the WRF-IFS-DA products. We

believe that demonstrating that only single members of the operational WRF suite properly capture this event in terms of its location, but not necessarily timing, is as scientifically significant as if all WRF configurations provided a good comparison against the observations. Furthermore, the new simulation is sufficiently capturing this thunderstorm event and therefore enables a deeper analysis of the physical processes inside and outside of the cloud. This discussion will be added to the revised manuscript.

Q11: 140: What does LAMPINET stand for?

A11: LAMPINET stands for the Lightning Network of the Italian Air Force Meteorological Service. This will be included in the revised manuscript.

Q12: 162: What does THUNDERR stand for?

A12: THUNDERR is an acronym of the project Detection, Simulation, Modelling and Loading of thunderstorm Outflows to design wind-safer and cost-efficient structures. THUNDERR is an abbreviation of THUNDERstorm that expresses the innovative Roar of this research. This description will be included in the footnote in the revised manuscript.

Q13: 221: Where are Querida I and II in Fig. 4a. I don't see Querida over northwestern Scandinavia but rather northeastern.

A13: This was a mistake, Querida is over northeastern Scandinavia indeed. Thank you.
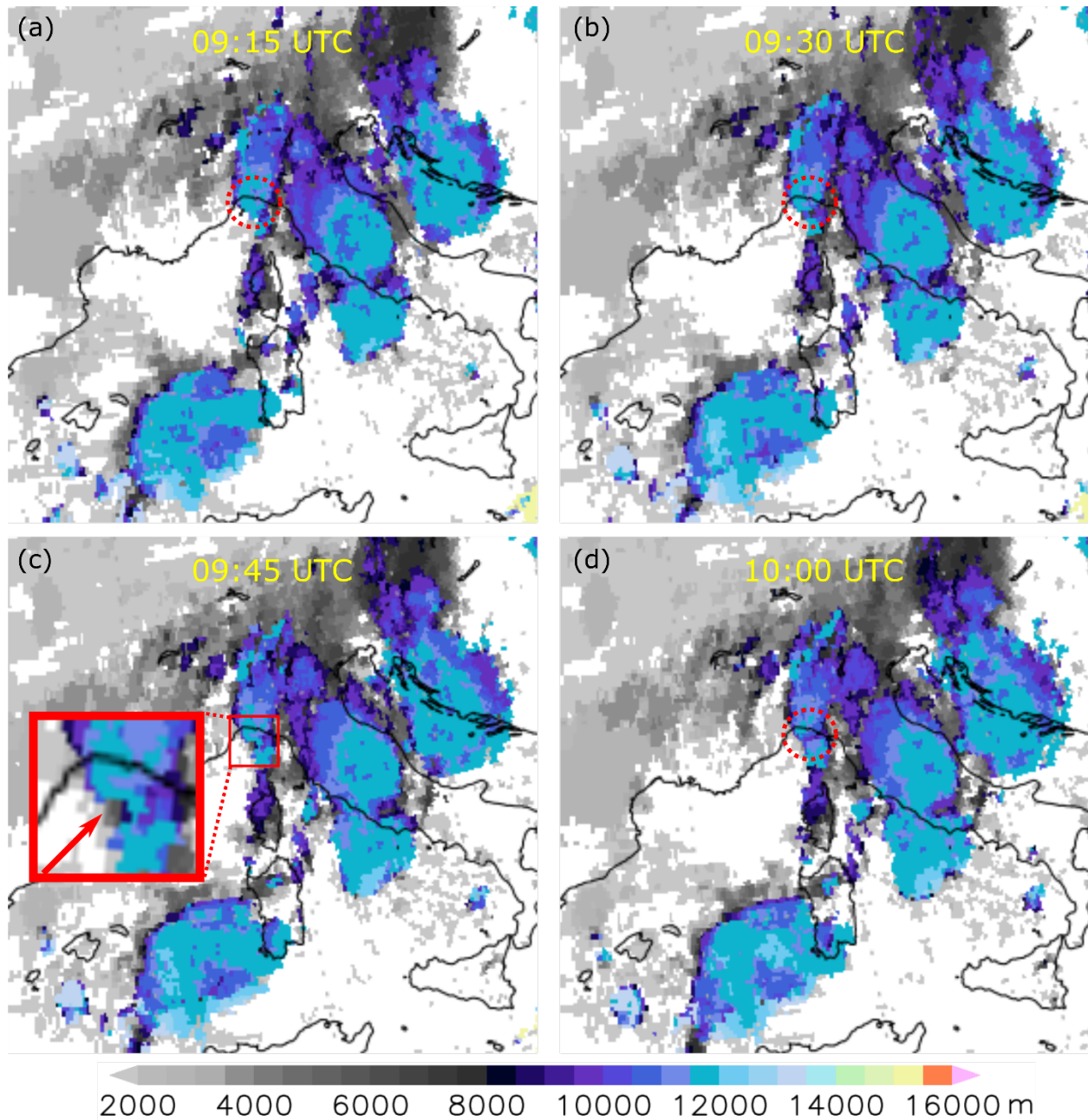
Q14: 233: I doubt that the connection of the two clusters over the sea is really relevant for the gust front observed at the coast.

A14: This analysis is looking at this thunderstorm system from a different (larger) scale. The goal here is not just to characterize the gust front and smaller-scale thunderstorm phenomena, but also to investigate the larger-scale weather scenarios that were associated with the thunderstorm development and propagation between 09:00 UTC and 10:00 UTC.

The connection between the thunderstorm development at the large scale and the gust front was not made in the manuscript, whereas this comment indicates that we have linked these two. So, we would like to clarify that too. Yet another goal of this analysis was also to show that this cloud system was slowly evolving and the cloud cover above the Genoa region stayed effectively unchanged throughout the collapse hour.

Q15: 237: The cloud tops above Genoa already reached 12.000 m at 09:15 UTC according to Fig. 5a.

A15: We thank the reviewer for this comment because we poorly expressed ourselves here. We did not want to say that some of the cloud tops were not at these heights prior to 09:45 UTC, but we wanted to say that the clouds were at 12,000 m at 09:45 UTC regardless of their previous top height. We will revise the sentence for clarity in the new manuscript. Kindly note that Figure 5c (below) now will also contain a zoom-in of the cloud tops above Genoa (also see our answer A16).

(a) 09:15 UTC
(b) 09:30 UTC
(c) 09:45 UTC
(d) 10:00 UTC

2000 4000 6000 8000 10000 12000 14000 16000 m

Q16: 241-248: The movement of the cells is not very visible in Fig. 6. The x- and y-axis range should be reduced. How do the radar images to the satellite observations? The shape of the cells is quite different. How can this be explained? What is the vertical structure of the cells? Instead of VMI the authors could show a MaxCappi.

A16: The range of *x* and *y*-axis will be reduced in Figure 6.

The radar data in Figure 6 are shown over a much smaller region than the satellite observations in Figure 5. However, both figures show that there is a small region of very shallow clouds south of Genoa. This area is now indicated with a red arrow in the new Figure 5c (see figure above in A15). This discontinuity is

5

also observed in the radar measurements in Figure 6. In addition, the pattern of radar reflectivity does not necessarily have to match the spatial pattern of could tops. An example is the Mesoscale Convective Complexes, in which case the cloud tops have a circular shape, but the radar reflectivity can resemble a squall line or different cloud cluster (Markowski and Richardson, 2010).

We do not have the vertical volume slices for this event in order to describe the vertical structure of cloud cells. The MAXCAPPI and few other radar products were excluded in order to have more space for other analyses in this manuscript. The reviewer also suggested that the number of figures could be reduced. Including a MAXCAPPI figure would only add more material and make the manuscript larger. Lastly, we believe that the presented radar products in terms of reflectivity (VMI) and surface rain intensities are sufficient for the analyses presented in this paper.

Q17: 248ff: I cannot distinguish the impact of orographic channeling on the precipitation cell. There is no observational evidence for this in the presented figures.

A17: The northeastern part of the VMI reflectivity in Figure 6 (VMI around 30 dBZ) follows the direction of the orographic valley. On the other hand, the orientation of the two cells that are located above the sea is zonal. The curvature in the VMI footprint in Figure 6 coincides with the location of the valley and it led us to propose that orography had an influence on cloud development. Of course, the orography, river valleys, and shorelines are the well-known contributors for cloud development and propagation.

We will implement this comment in the revised manuscript by stating that it is likely the orography influenced the cloud propagation.

Q18: 258: The SRI images in Fig. 7 are rather redundant to Fig. 6. How are the translation velocities calculated, i.e. how is the arrow drawn in the figure at 09:00 UTC calculated?

A18: This figure shows the rain intensity while Figure 6 is the radar reflectivity. We argue that Figure 7 is complementary to Figure 6 and not redundant.

The arrow in Figure 7 uses the direction and magnitude of the speed of the rain cell centroid derived in the following way.

The 5-min Surface Rainfall Intensity (SRI) estimates were obtained from the national mosaic of the Italian Meteo Radar Network (see http://www.protezionecivile.gov.it/risk-activities/meteo-hydro/activities/prediction-prevention/central-functional-centre-meteo-hydrogeological/monitoring-surveillance/radar-map for examples and additional details) and were used to identify the storm cell movement towards the coast in the period from 9:00 to 9:55 UTC on 14 August 2018.

The cell was isolated from the rest of the precipitation field observed at the national scale through the application of a region growth algorithm to the binary image rain/no rain (Gonzalez and Woods, 2002). For each time step, t_i, the centre of mass of the precipitating cell was identified and the module, v_{t_i}, and direction, θ_{t_i}, of the cell were calculated by:

$$v_{t_i} = \frac{|\vec{r}_{t_{i+1}} - \vec{r}_{t_i}|}{\Delta t}$$

$$\theta_{t_i} = \tan^{-1}\left(\frac{x_{t_{i+1}} - x_{t_i}}{y_{i+1} - y_{t_i}}\right).$$

Here, $\vec{r}_{t_i} = (x_i, y_i)$ is the position vector of the cell centroid with the longitude, x, and the latitude, y, in meters.

Q19: 264: north-eastward!

A19: Thank you for spotting this inaccuracy. It will be corrected in the revised manuscript.

Q20: 265ff: The evolution of the cell in Fig. 7 does not agree with the statement in l. 263-264 that the cell is more compact over orography.

A20: The cell is not more compact over land, but we observe that it gets elongated in the direction of the valley after it makes its landfalls at Genoa. A similar pattern of elongation is also observed in the reflectivity data in Figure 6. We do agree that Figure 6 and 7 do not look identical, but it is expected because they are not portraying the same quantity. This is an additional reason for keeping both figures in the manuscript.

Q21: 272-274: The lightning distribution does not fit to the reflectivity images in Fig. 7. Please explain.

A21: It is not clear to us what the reviewer refers to with the following statement: "The lightning distribution does not fit the reflectivity…" The Blitzonturg imagery of lightning seems to follow nicely the meridional orientation of cloud tops that were also captured in the satellite images. On the other hand, the lightning captured by the LAMPINET network is mostly located south to southeast from the bridge (northeastward motion of the lightning zone). Note that the LAMPINET imagery is only a subset of the Blitzonturg data that covers a much larger region. The northeastward propagation of the lightning zone is similar to the overall propagation of the precipitation zone in Figure 7—i.e., both are predominantly northeastward.

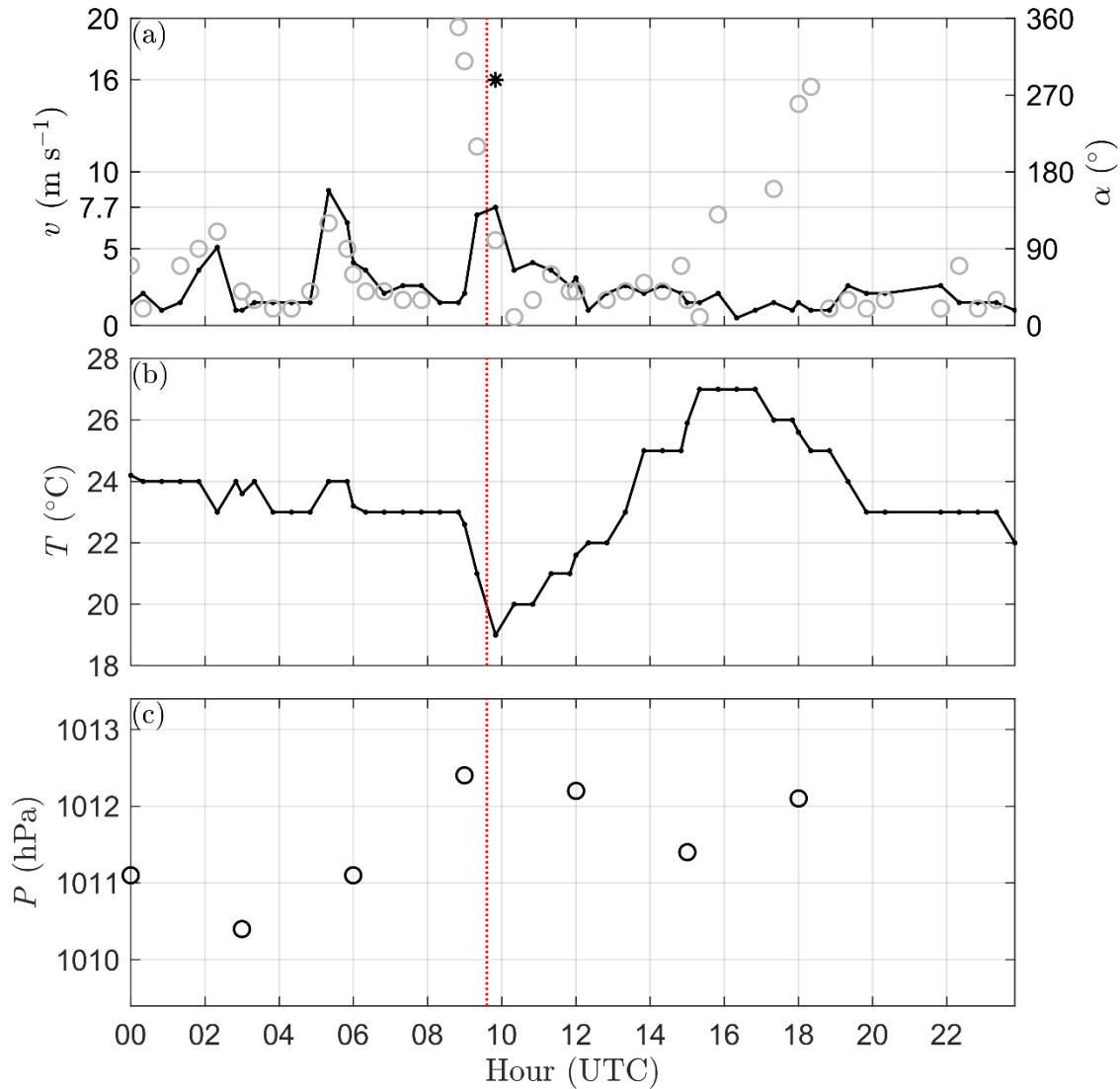**Q22:** 281-282: This is in contradiction to the stdatement on lightning in the introduction.

A22: We have clarified this part because we believe it is very important for the paper. In Line 41 it is stated that "the lightning occurred to the east-southeast of the bridge", not over the bridge, and this is coherent with the statement in lines 281-282, as also already explained in the previous answer A2.

Q23: 287ff and Fig. 9: Wind direction should be plotted as markers and not as a connected line as this is misleading. Markers should also be added to temperature and wind speed as the temporal resolution is low. Wind direction might as well change over north. This is not clear from this measurement as the temporal resolution is too low. How does the northerly wind observed at the surface fit to the northward propagation of the cells? Why is temperature not shown for all stations where it is available (Tab. 1). It would be very interesting to see the spatial distribution of the drop in temperature.

A23: Wind direction is now plotted as markers. Markers are also added to temperature and wind speed time series. The markers now show that the wind direction was indeed changing in the counterclockwise direction in the interval centered on the collapse time (between 08:50 UTC and 10:20 UTC). This will be clarified in the manuscript text too.

The wind direction at and around the bridge collapse time was not from the north. The wind direction was 140° (southeast). In relation to the bridge collapse hour, the northern winds are only observed around 08:50 UTC and around 10:30 UTC.

Air temperature is not shown for all stations in order to shorten the manuscript and reduce the total number of figures. Moreover, also the other temperature measurements are unfortunately available every 30 min and such a low temporal resolution does not allow to add any relevant information concerning the gust propagation. These changes are shown in the revised figure below.

Q24: 308: I do not see a subsequent increase in pressure.

A24: The maximum value of surface pressure was observed close to the bridge collapse time (Fig. 9c). Unfortunately, the time resolution of pressure data is even lower than temperature and wind data, but nevertheless, we do observe the peak in surface pressure at 09:00 UTC. In addition, it is logical to assume that the pressure did not plateau after 09:00 UTC and immediately started dropping to the next observed value at 12:00 UTC.

Moreover, the gust front theory proposed by Wakimoto (1982) and later nicely depicted in Markowski and Richardson (2010) demonstrates that the pressure rise associated with the thunderstorm (i.e., gust front) passage is slower than the abrupt changes in air temperature or wind velocity. For instance, see Figure 5.23 from Markowski and Richardson (2010).

Q25: 318: How are hail and graupel distinguished at the weather stations?

A25: There was no need to distinguish between hail and graupel because no ice particles were observed at the surface. We have rephrased this sentence to read as follows: "No hail or any other ice particles were observed in this period at the weather stations in the Genoa region."

Q26: 320ff: Be more specific. Station 11 shows westerly wind and stations 9 and 8 show southerly wind. For a clearer presentation of the spatial distribution of wind the authors could show a spatial map with the wind plotted as arrows at the individual sites for specific times before, during and after the downburst.

A26: New pictures/panels will be added to Fig. 11 (not to increase the overall number of figures) with the wind plotted as arrows. We didn't do it before because we thought the explanation of Fig. 11 was clear enough, but probably this was not the case, so it is worth adding new pictures as suggested by the Reviewer.

Q27: 352: Note the recent study of Pantillon et al. (2019) on the observational detection of downbursts with Doppler lidar.
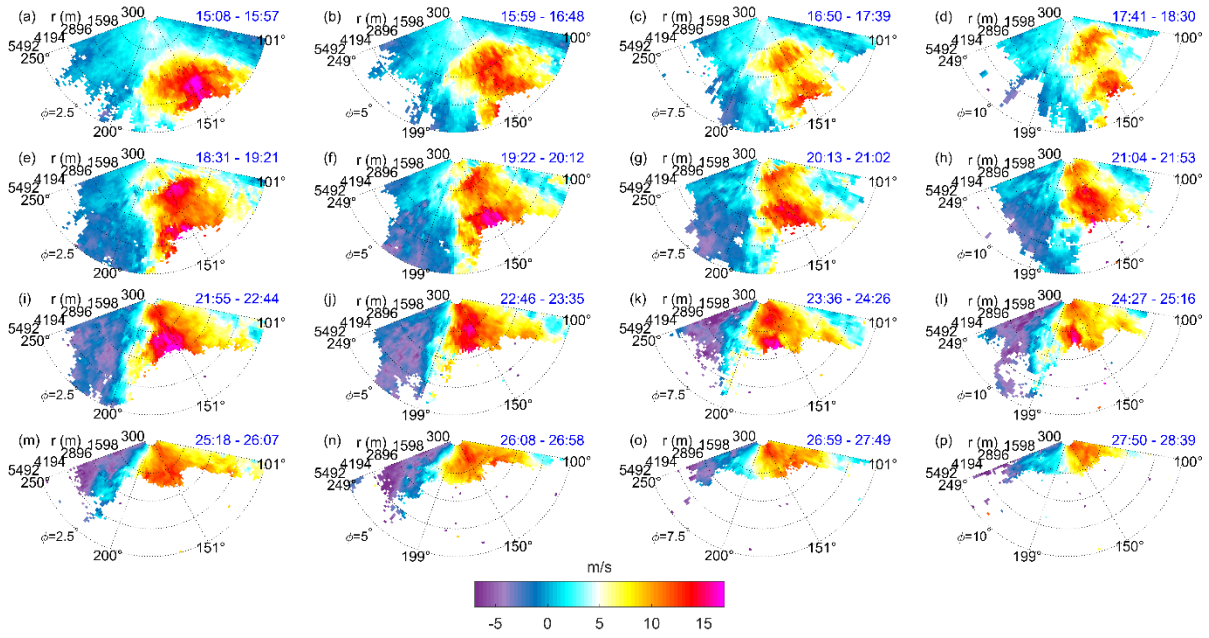
A27: This paper will be cited in the revised manuscript. We thank the reviewer for suggesting the relevant literature.

Q28: 358: How is the region with maximum velocity identified? Did the authors use an objective method?

A28: The region with the maximum velocity is identified by inspecting raw lidar measurements. We did not use any particular mathematical tool in this process because it is obvious from figures and data (numbers) where the high-velocity zones are.

Q29: Fig. 12: This figure needs to be much improved. The shown range has to be adapted to the actual measurement range and color range also needs be decreased. The coast line should be added and maybe even the surface measurements at the caostal stations. The time stamp format is confusing. Is it really necessary to show the seconds?

A29: Figure 12 is now improved. The color bar range now represents the real measurements and it is spanning from -7 m s^{-1} to $+17$ m s^{-1}. The radial extent is also reduced in order to show better resolution of valid lidar measurements. The radial distance is now limited to 5492 m away from the lidar because the data beyond that radius are either unreliable or non-existent due to precipitation. In addition, this figure is now saved at a much higher resolution (600 dpi). The modifications are shown in the figure below, but kindly note that the figure is made to be inserted on a landscape page (not a portrait page as in this document).

The color scheme employed in this figure was specifically designed for lidar measurements. The cool colors are associated with negative Doppler velocities (i.e., away from lidar), whereas the warm colors are showing positive Doppler velocities (i.e., towards lidar). The white color shows 0 m s^{-1} Doppler velocities. We believe that this color scheme is rather intuitive and helps in fast identifications of positive and negative velocity zones. The surface measurements at the coastal stations are already shown in Fig. 11.

When it comes to the coastline, Fig. 2 shows that the lidar is located at the tip of the coastline and effectively over the sea. The azimuth range is from 101° to 250° and it never crosses the coastline. In order to facilitate this comment, we will add the lidar scanning area to Figure 2.

The flow field evolution and the scanning pattern of the lidar are on the time scales of a minute or so. Therefore, we decided to leave the exact times—including seconds—as the lidar software outputs them. It just increases the precision of the reported data. Instead of HH:MM, we present HH:MM:SS, so we do not see the addition of seconds makes these plots more confusing. Since the entire range of observations in Fig. 12 is taking place at 09:MM:SS, we have decided to remove 09 from the label.

Q30: 361ff: It is important to realize that radial velocity is measured by the lidar. This means that the three-dimensional wind vector is projected on the direction of the lidar beam. For example, southerly wind cannot be detected at easterly azimuth angles. This means that the front could be wider, but not be detected anymore by the lidar due to a changing azimuth angle. Also, the decrease of radial velocity at larger elevation angles could be related to a changing wind direction. Overall, the problems and difficulties related to radial velocity measurements need to be much more discussed.

A30: The authors are aware of the limitations of lidar measurements and we agree with the reviewer's observations regarding the gust front width. We will correct this statement in the revised manuscript. Indeed, the change of radial velocity could partially be due to the wind direction change with height. However, the changes in the heights between two elevation angles are below 100 m and it is not likely that the wind direction changes drastically in such a shallow layer. In addition, it is not clear from this

comment to which statement on the radial velocity decrease in our manuscript the reviewer is referring to. We have stated that the zone of the high wind speeds is closer to the lidar at the higher elevations.

Q31: Fig. 13: How is it possible that eight gust front heights are given in Fig. 13, while only 7 are indicated in Fig. 12? From which elevation angles is the displacement velocity determined? The contribution of the horizontal wind to the radial velocity is different at different elevation angles. Could this play a role in the estimated gust front heights, i.e. why is the gust front at 7.5 degree always higher than at 10 degree?

A31: Only seven gust fronts are indicated in Fig. 12 because the front is above lidar around the time instant that corresponds to Fig. 12h (09:21:04–09:21:53 UTC). Even in Fig. 12g the dotted line is very short.

We agree that the contribution of horizontal wind speed to the radial velocity is different at different elevations. The methodology for obtaining Fig. 13 is as follows. Firstly, we determine the distance between the lidar and the gust front edge (D_f) at different elevations by inspecting the raw lidar data (Doppler velocities). Then, we project that distance that is along the lidar beam to the horizontal plane (X_f) as:

$$X_f = D_f \cos \varphi,$$

where φ is the elevation angle. Similarly, the height of the gusts front edge above the lidar (H_f) is determined as:

$$H_f = D_f \sin \varphi.$$

Note that the values of X_f and H_f are available for two consecutive scans of the four elevation angles (Fig. 12a–h). We call them X_{fs1} and X_{fs2}, and H_{fs1} and H_{fs2} for scans 1 and 2, respectively.

Then, the horizontal displacement velocity of the gust front (V_{disp}) at two different heights is calculated as:

$$V_{disp} = \begin{cases} \dfrac{X_{fs1}^{\varphi_1} - X_{fs2}^{\varphi_3}}{6T_b}, & \text{at 115 m,} \\[2mm] \dfrac{X_{fs2}^{\varphi_1} - X_{fs2}^{\varphi_4}}{3T_b}, & \text{at 70 m.} \end{cases}$$

Here, the superscript indicates the height at which the horizontal distance is considered and $T_b = 51$ s is the scanning time of lidar (49 s of scanning per elevation plus 2 s of moving to the next elevation angle). These quantities are plotted in Fig 13. Our results show that these two displacement velocities are similar (Fig. 13 and also discussed in the revised manuscript). As demonstrated above, V_{disp} is estimated as the function of geometric variables and not radial (Doppler) velocity along the lidar beam.

Q32: 398-400: From which station are the surface measurements taken? Are the values similar when using the other stations measuring temperature (Tab. 1)?

A32: The surface measurements are taken from the Genova Airport (i.e., Genova Sestri) weather station. Some of the stations in Table 1 do not record temperature, pressure, and relative humidity (e.g., GEPOA, GEPWA, etc.). Therefore, these stations cannot be used in this analysis.

We have chosen Genova Airport station because it is a registered World Meteorological Organization (WMO) weather station located at the Genoa airport (USAF number 161200) and, in addition, it is the

weather station that is the closest to the coastline. Similar to the lidar, it is effectively measuring the atmospheric conditions above the sea in the cases when the wind direction is from the sea towards the land (as it was in the analyzed case).

The results are not the same if other weather stations are used, but this is expected as the other stations are at higher elevations in comparison to the lidar and Genova Airport sites. Nevertheless, most of the other weather stations in Genoa recorded the minimum temperature around 19°C, but the temperature prior to the thunderstorm gust front passage was not necessarily 23°C, but lower. This indicates that the passage of the gust front was similarly observed at all stations. The air temperature prior to the gust front was lower at other stations because these stations are located at higher altitudes in comparison to Genoa Airport. Indeed, this is one of the major reasons for using the Genoa Airport station (i.e., the same altitude as the lidar, which is effectively the sea level). That is, the elevation of Genoa Airport is 3 m above sea level, whereas the lidar is at 5 m above sea level. The other stations in Table 1 are at much higher elevations. We will add these clarifications to the revised manuscript.

Q33: 408-409: The values in Charba (1974) were very different compared to the ones found in the present study. It would be worth discussing the different atmospheric conditions under which the gust fronts occurred.

A33: Indeed, the values in Charba (1974) significantly differ from our values and this was one of the reasons for reporting it in this paper. We would like to emphasize that the methodology presented above (e.g., related to the reviewer's comments Q31 and Q32, and similar) is not proposed and developed to provide the exact values of gust front displacement velocity or vertical structure, but an approximation of these values based on the limited data that are available. Excluding the lidar data, the other data used in this methodology are readily available from standard meteorological measurements.

Charba (1974) analyzed a gust front that occurred on 31 May–1 June 1969 over Oklahoma and Kansas, United States (US). He reported the air temperature drop of about 5°C (25°C to 20°C) and a pressure increase of 0.2 inches of Hg, which corresponds to approximately 677.3 Pa (~6.8 mb). We observe that both temperature and pressure drop in their case was higher than in our study—in particular the pressure drop differences. However, the temporal resolution of our pressure measurements is lower than the resolution of temperature measurements, so the pressure jump in our case could have been higher than the reported value. This is an uncertainty that we clearly reported in Fig. 9. We will add some additional discussion on our results and their similarity to Charba (1974).

However, we kindly emphasize here that Mueller and Carbone (1987) observed the similar value of gust front displacement velocity (i.e., 6.9 m s^{-1}) in their study on the dynamics of thunderstorm outflows in the US. We have reported this similarity between the two studies in the original manuscript. Similarly, the manuscript reports the similarity between our results and Goff (1976), as well as Mueller and Carbone (1987).
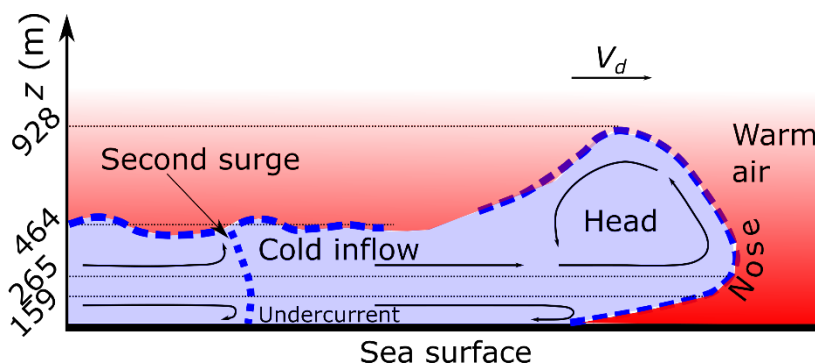
Q34: 420-421: Here the authors state that the wind speed increases with height in the outflow. However, radial velocity decreases with increasing elevation angle, i.e. with height according to the detected gust front heights (Fig. 13). Please explain.

A34: Our answer A31 above described the methodology for obtaining the approximate heights of the gust front and its displacement velocity in the direction of the lidar. We have also emphasized now that the

obtain displacement velocity of the gust front is the projection of the overall displacement velocity in the direction of the lidar. Radial velocity is not always decreasing with height (Fig. 12). Quite the opposite, the radial velocity is usually increasing with height above a fixed point. As an example, we fix the point at the radius of 1598 m from the lidar and azimuth of 151°, and we analyze the four different elevation angles in Fig. 12a–d. The radial velocity is clearly increasing with the height (i.e., with increasing elevations). While there are some regions in the flow where the radial velocity is decreasing with height, these are fewer in comparison to the opposite.

Q35: 449-450: Where can the two regions with high wind speed be found in Fig. 14?

A35: The first region of high wind speed is associated with the leading gust front head, while the second region is located behind the dotted line that indicates the second surge of the cold air that outflows from the thunderstorm. This schematically representation is also in accordance with the gust front outflow model proposed by Charba (1974) in Fig. 11 in his paper. That is, the cold outflows are not necessarily continuously spreading below and in front of the thunderstorm, but rather in a series of surges. We will discuss further this process in the revised manuscript, but note this was also included in the original version of this manuscript. In addition, we have added an arrow and explanation of the second surge in Fig. 13.
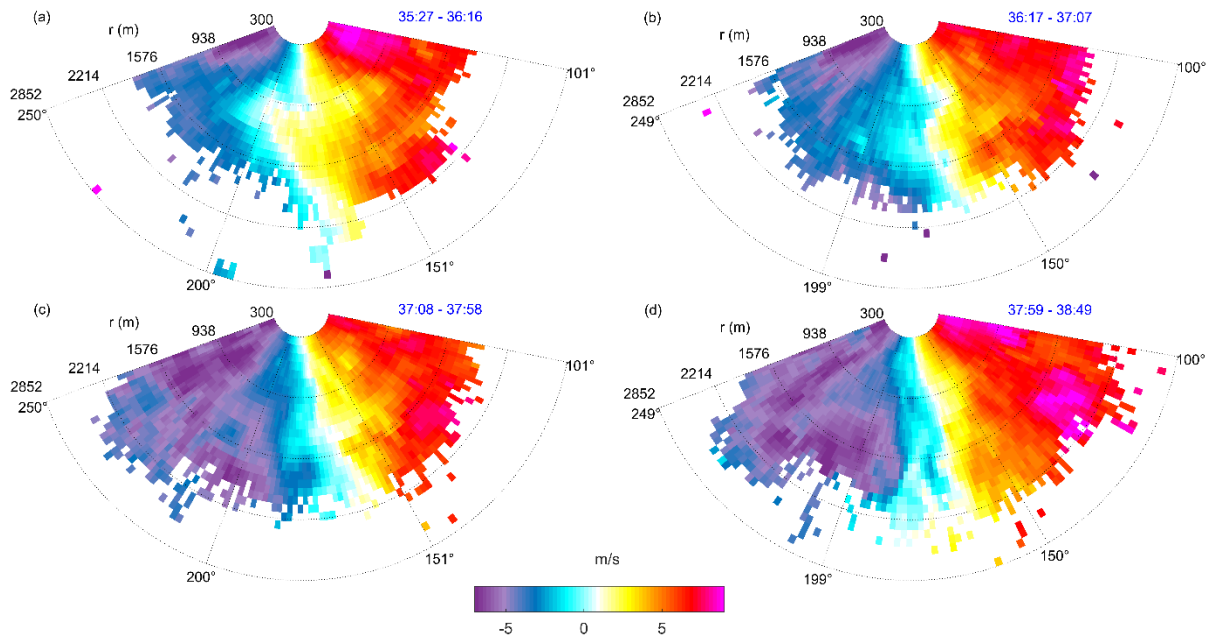

Q36: 451-452: "decreases with time": At which stage of the gust front? Prior or after the the maximum of the gust front was reached? Distances given are along the beam? This needs to be converted to horizontal distance which is different for different elevation angles. According to Fig. 13 the gust front height is largest for 7.5 degree elevation angle (and not 10 degree). According to this the distance would decrease with height. This whole issue needs to be analyzed more carefully paying more attention to horizontal and along beam distances and height compared to elevation angle.

A36: This sentence is now removed from the revised manuscript. The observation was based on Fig. 12, which shows the results along the beam. The distances between two high-regions in Fig. 12a–d seems to be a bit larger than in the corresponding panels in Fig. 12e–h. However, the closer analysis shows that the decrease is either very small or in some cases not obvious. In order to remove any confusion related to this point, we have decided to remove this part from the revised manuscript.

Q37: 463-464: How does this easterly wind detected by the Doppler lidar relate to the surface measurements? How does it relate to the northward propagation of the gust front. Please discuss!

A37: This result is in accordance with the cell movement in Fig. 7. The precipitation region was advancing in the northeastward direction and after 09:40 UTC the precipitation zone was located east of the lidar.

Q38: 475-476: Which two peaks? There are no peaks visible in WRF-GFS and WRF-GFS-DA in Fig. 16. Why is the period confined to 08:30 and 09:55 UTC? Why not before 08:30 UTC when the wind speed was just as high in WRF-IFS? How does the wind direction in the model compare to the observed ones?

A38: We have now added the same plot for the WRF-IFS-DA (Figure B in A10). This experiment shows a clear wind gust peak of 12–13 m s^{-1} at 11–12 UTC at the anemometers' locations. Moreover, the predicted wind directions in WRF-IFS-DA simulation are in good agreement with the observations.

Q39: 487-490: The storm at 13:25 UTC in the observations also fits to the storm in WRF-IFS at that time.

A39: On 14 August 2018, in the morning there were many convective cells that developed off the coast of Genoa. When looking at all the available time-frames of radar observations (every 10 minutes, not shown in the paper), it is apparent that the two cells in Fig. 17b are the evolution of the larger convective structure shown in Fig. 17a, whereas the two cells shown in Fig. 17c are new cells independent from the previous ones. That being said, we compared the convective structure simulated by WRF-IFS at 12:40 UTC to the one observed at 8:30 UTC just because they are similar in terms of shape, size and position, while the match between WRF-IFS at 12:40 UTC and observations at 13:25 UTC is weaker, in our opinion. However, this does not mean that WRF-IFS at 12:40 UTC and observations at 8:30 UTC are the same convective phenomena and the Reviewer is right saying that the simulated one is also similar, to some extent, to the storm at 13:25 UTC. This will be further clarified in the revised paper.

Q41: 491ff and Fig. 18: Why is the thermodynamic diagram calculated for the grid point in the center of the cell? Thermodynamic diagrams are usually used to describe the pre-convective or post-convective environment and not the conditions within the cell. If the grid point shown in Fig. 18 is within the cell, why is there no saturation?

A40: The thermodynamic diagram was not calculated for the grid point in the center of the cell. Conversely, it was computed in the region affected by the convective cells transition. However, the diagram is now substituted by the one computed from the WRF-IFS-DA run.

Q42: 506ff: The analysis of the simulations is rather superficial and at least for the WRF-IFS run which is able to produce some storms in the area a comprehensive evaluation of the model output for temperature and wind should be performed and the shape and existence of a potential gust front should be analysed. I cannot follow the conclusions the authors draw from the model simulations, e.g. I do not see a potential of the WRF runs to provide precursors for storms as two of three simulations fail to produce any kind of storm and the third simulation represents it at the wrong time.

A42: The new simulation is added to complete the set of these figures. The WRF-IFS-DA results show a gust front propagation (see Figure C below) in the period between 11:00 and 11:55 UTC (every 5 minutes). We agree with the reviewer that the model simulations are not able to perfectly reproduce the timing and location of the observed event. However, these simulations are performed in an operational framework and the location and timing error is in line with the state-of-the-art numerical weather modelling prediction of these types of convective events. Furthermore, even with somewhat different timing and location of the event, the WRF-IFS-DA simulation is reproducing the thunderstorm cloud well enough to be used to get a deeper insight into the physics of this event (e.g., analyzing processes that are not obtainable from a surface or remote sensing measurements such as microphysics processes and species).
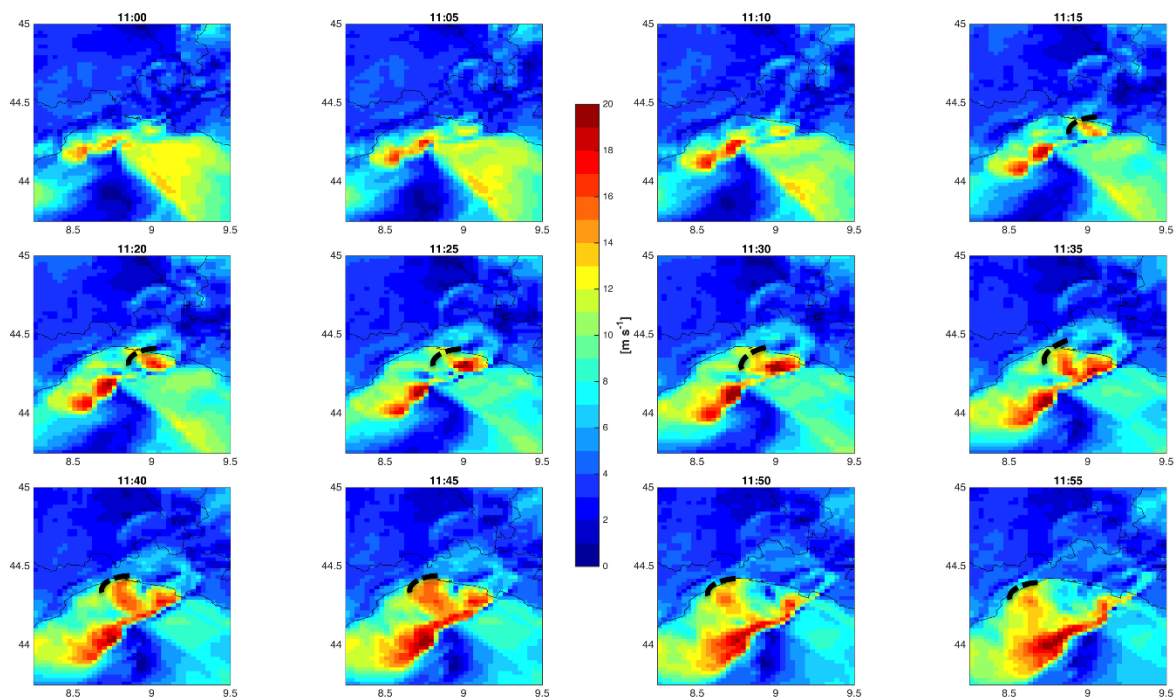

Figure C: Maximum 10-m wind speed (wind gust) at 5-min temporal resolution in the time period 11:00–11:55 UTC from the WRF-IFS-DA simulation.

As an example, Figure D shows a vertical cross-section of the reflectivity field at 11:30 UTC for the WRF-IFS-DA experiment. Severe convection is apparent in front of Liguria coastlines in association with a well-

organized system of updraft and downdrafts. This system produces near-surface wind gusts that propagate from the south-east (Figure E).

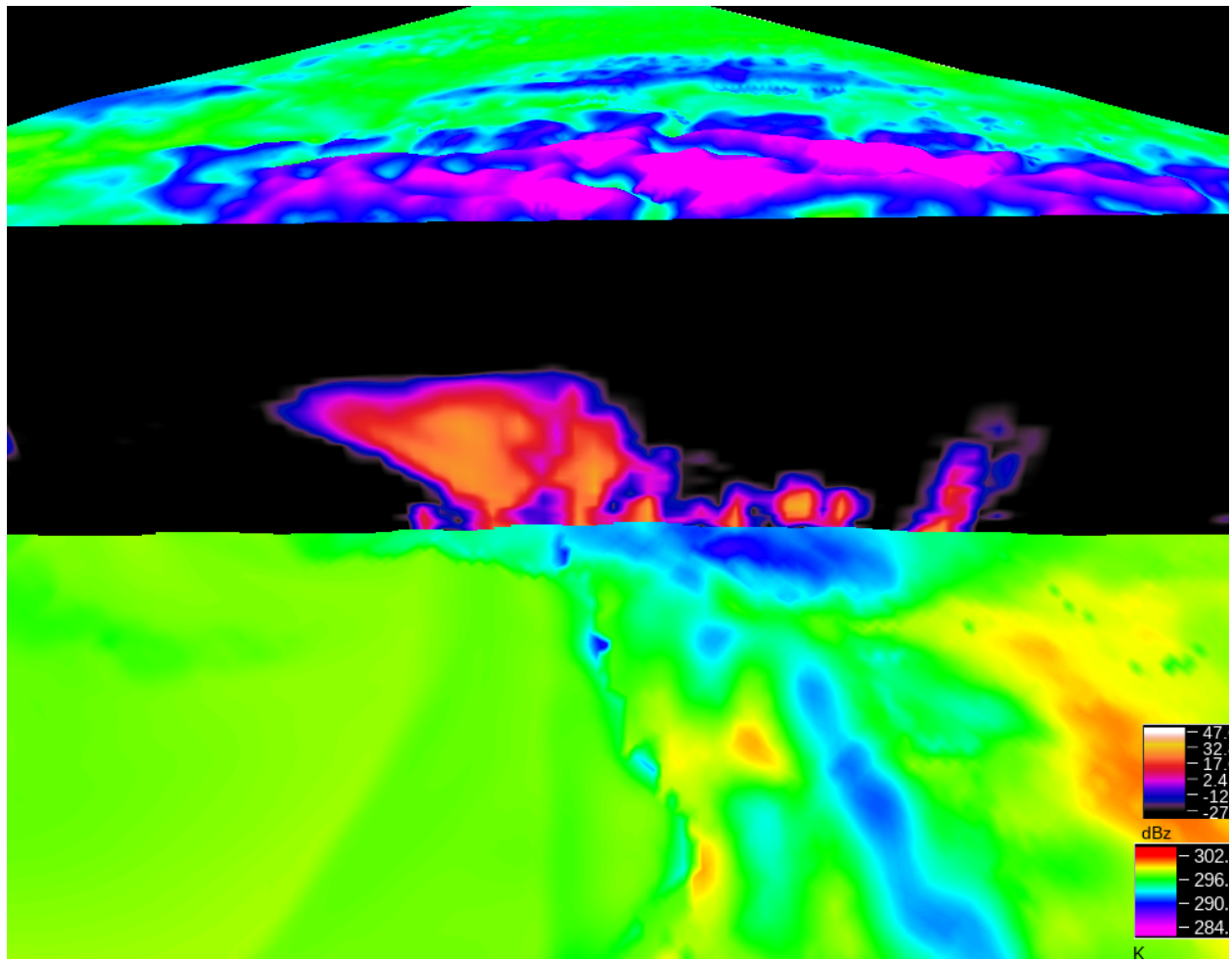A comprehensive description of this new simulation will be reported in the revised manuscript.

Figure D: Vertical cross-section of the WRF-IFS-DA simulated radar reflectivity along the convective cell developing in front of Liguria coastlines at 11:30 UTC. The shaded colors in the horizontal plan show the air temperature at 2 m above ground.
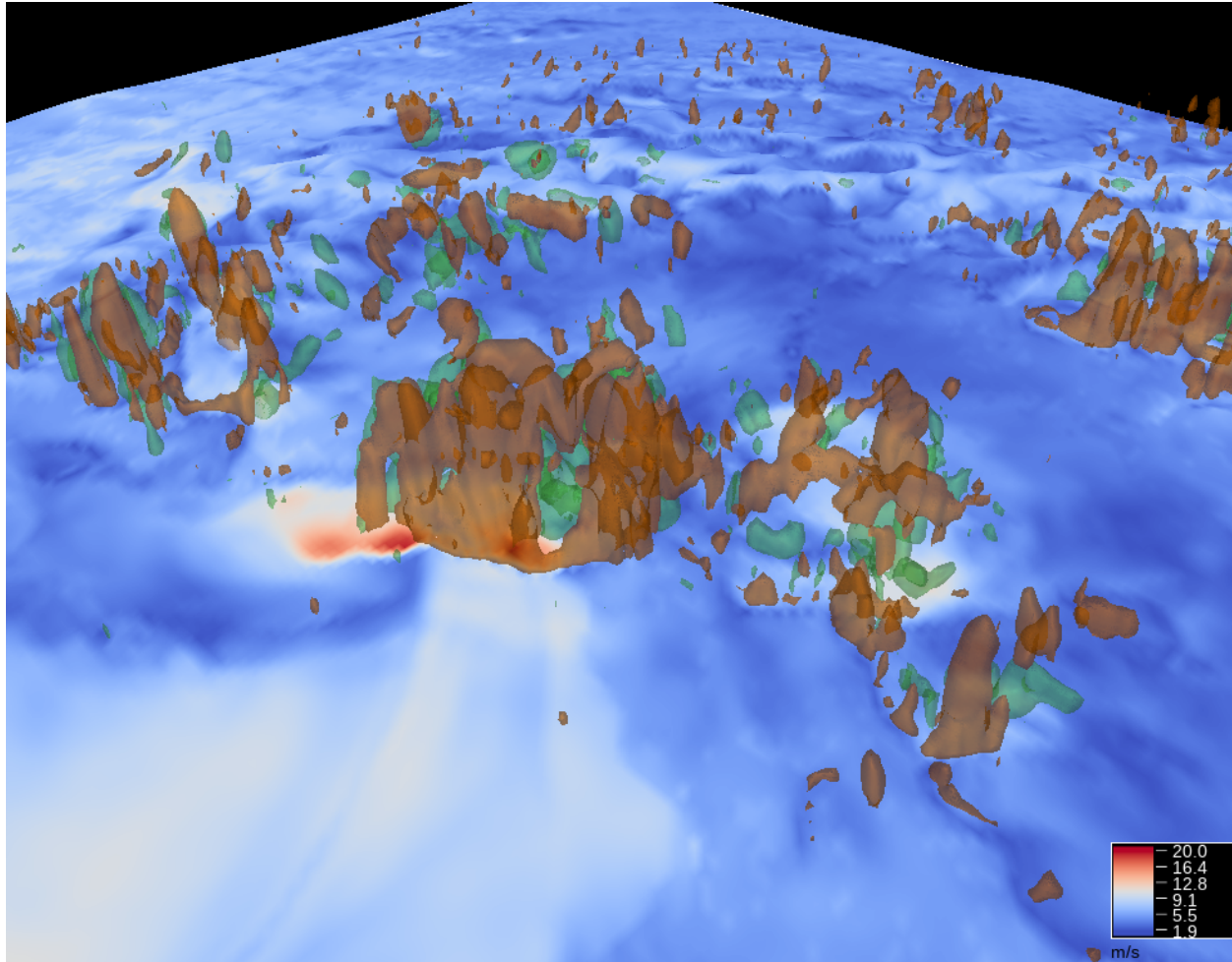
Figure E: Updrafts (+1 m s^{-1} red isoline) and downdrafts (-1 m s^{-1} green isoline) in front of Liguria coastlines at 11:30 UTC from the WRF-IFS-DA simulation. The wind gust at 10-m above ground field is also shown in shaded colors.

Supplementary references

Charba, J.: Application of gravity current model to analysis of squall-line gust front, Mon. Wea. Rev., 102(2), 140–156, doi:10.1175/1520-0493(1974)102<0140:AOGCMT>2.0.CO;2, 1974.

Drobinski, P., Ducrocq, V., Alpert, P., Anagnostou, E., Béranger, K., Borga, M., Braud, I., Chanzy, A., Davolio, S., Delrieu, G., Estournel, C., Boubrahmi, N. F., Font, J., Grubišić, V., Gualdi, S., Homar, V., Ivančan-Picek, B., Kottmeier, C., Kotroni, V., Lagouvardos, K., Lionello, P., Llasat, M. C., Ludwig, W., Lutoff, C., Mariotti, A., Richard, E., Romero, R., Rotunno, R., Roussot, O., Ruin, I., Somot, S., Taupier-Letage, I., Tintore, J., Uijlenhoet, R. and Wernli, H.: HyMeX: A 10-year multidisciplinary program on the MediterraneanwWater cycle, Bull. Amer. Meteor. Soc., 95(7), 1063–1082, doi:10.1175/BAMS-D-12-00242.1, 2013.

Goff, R. C.: Vertical structure of thunderstorm outflows, Mon. Wea. Rev., 104(11), 1429–1440, doi:10.1175/1520-0493(1976)104<1429:VSOTO>2.0.CO;2, 1976.

Gonzalez, R. C. and Woods, R. E.: Digital Image Processing, 2nd edition, Prentice Hall, Upper Saddle River, N.J., 2002.

Grasso, L. D. (2000). The differentiation between grid spacing and resolution and their application to numerical modeling. Bull. Amer. Meteor. Soc., 81(3), 579-580.

Markowski, P. and Richardson, Y.: Mesoscale Meteorology in Mid-Latitudes, John Wiley & Sons, Ltd, Chichester, United Kingdom., 2010.

Mueller, C. K. and Carbone, R. E.: Dynamics of a thunderstorm outflow, J. Atmos. Sci., 44(15), 1879–1898, doi:10.1175/1520-0469(1987)044<1879:DOATO>2.0.CO;2, 1987.

Wakimoto, R. M.: The life cycle of thunderstorm gust fronts as viewed with Doppler radar and rawinsonde data, Mon. Wea. Rev., 110(8), 1060–1082, doi:10.1175/1520-0493(1982)110<1060:TLCOTG>2.0.CO;2, 1982.